# Experimental and Theoretical Studies of Elemental Site Preferences in Quasicrystalline Approximants (R-Phases) within the Li−Mg−Zn−Al System

**Chi-Shen Lee and Gordon J. Miller***

Department of Chemistry, Iowa State University, Ames, Iowa 50011-3111

*Received July 25, 2000*

A series of ternary and quaternary R-phase compounds in the Li−Mg−Zn−Al system are synthesized from pure elements in sealed Ta tubes with starting compositions based on the suggestions from electronic structure calculations using relative Mulliken populations to quantify the site preferences for the various elements. Single-crystal structural analyses reveal new R-phase compounds with various Li/Mg and Zn/Al ratios. The space group of all compounds is $Im\bar{3}$ (No. 204). Five quaternary phases [$Li_{1.00(1)}Mg_{0.63(2)}Zn_{1.23(1)}Al_{2.14(1)}$ (**1**), $a = 14.073(3)$ Å; $Li_{1.00(1)}Mg_{0.63(1)}Zn_{1.42(1)}Al_{1.96(1)}$ (**2**), $a = 14.088(3)$ Å; $Li_{1.01(1)}Mg_{0.62(1)}Zn_{1.31(1)}Al_{2.06(1)}$ (**3**), $a = 14.096(5)$ Å; $Li_{1.03(1)}Mg_{0.60(1)}Zn_{1.78(3)}Al_{1.59(3)}$ (**4**), $a = 13.993(5)$ Å; $Li_{0.78(2)}Mg_{0.85(2)}Zn_{2.47(1)}Al_{0.94(1)}$ (**5**), $a = 13.933(2)$ Å] and four ternary compounds [$Li_{1.63}Zn_{0.81(1)}Al_{2.56(1)}$ (**6**), $a = 14.135(3)$ Å; $Li_{1.63}Zn_{1.42(1)}Al_{1.95(1)}$ (**7**), $a = 13.966(5)$ Å; $Li_{1.63}Zn_{1.59(1)}Al_{1.78(1)}$ (**8**), $a = 13.947(2)$ Å; and $Li_{1.63}Zn_{1.77(1)}Al_{1.60(1)}$ (**9**), $a = 13.933(4)$ Å] are identified. The crystal structure exhibits an Al/Zn (M sites) network constructed from $M_{12}$ icosahedra and $M_{60}$ buckyball-type clusters. Li/Mg atoms (A sites) fill cavities within the Al/Zn network to give pentagonal dodecahedra ($A_{20}$). The site-potential studies (relative Mulliken populations) indicate two groups of atomic sites (positively and negatively polarized), which are consistent with the single-crystal studies. Further differentiation of site potentials among the various electropositive sites leads to segregation of Li and Mg, which is also verified experimentally. The analysis of relative Mulliken populations in an intermetallic framework provides a useful method for elucidating elemental site preferences when diffraction techniques cannot unequivocally solve the site preference problem.

## Introduction

Quasicrystalline phases are a young class of solid-state compounds that exhibit noncrystallographic rotational symmetries in their diffraction patterns.[1−3] Compositions (including phase widths), structures, and physical properties have been studied intensively for a variety of quasicrystalline phases in binary and ternary intermetallic systems.[4−7] To date, however, the actual structures of most quasicrystals are still a mystery. On the other hand, some crystalline intermetallic compounds are considered "quasicrystalline approximants" because their building blocks contain high-symmetry polyhedra that can be used as possible models for components of quasicrystalline structures.[2,3,8−10] One of these quasicrystalline approximants is the $Mg_{32}(Zn,Al)_{49}$ structure type (also called the R-phase structure, Pearson symbol cI160), which was first reported by Bergman and Pauling.[8,9] Its structure features a network of fused polyhedra with icosahedra, pentagonal dodecahedra, and truncated icosahedra ($C_{60}$-type cages). This particular structure type is only found in ternary or higher order intermetallic systems.[11−16]

We recently reported a detailed, systematic investigation of the phase width, elemental site preferences, physical properties, and electronic structure of the ternary Mg−Zn−Al R-phase system.[11] According to our results, the seven crystallographic sites in the R-phase structure can be separated into three distinct sets: (1) three sites (52 atoms per unit cell) exclusively contain the electropositive Mg atoms (we will call these A sites: A1, A2, A3); (2) three sites (96 atoms per unit cell) have mixtures of Zn and Al atoms (we will call these M sites: M1, M2, M3); and (3) one site, called M4 (12 atoms per unit cell), contains a mixture of Zn and Mg atoms with ca. 33% vacancies. Electronic structure calculations can rationalize the observed phase width in this system due to a region of M−M nonbonding levels in the densities of states (DOS) occurring over a range of valence electron concentrations (vec's) between ca. 2.1 and 2.3 (vec = the total number of valence electrons divided by the total number of atoms in a formula unit). Vacancies occur in the Mg−Zn−Al R-phases because the observed compositions set vec values that lead to the occupation of some M−M antibonding levels when all sites are completely occupied. This explanation of vacancies in an intermetallic system is similar to the Grimm−

(1) Shechtman, D.; Blech, I.; Gratias, D.; Cahn, J. W. *Phys. Rev. Lett.* **1984**, *53*, 1951−1953.
(2) Goldman, A. I.; Kelton, R. F. *Rev. Mod. Phys.* **1993**, *65*, 213.
(3) Janot, C. *Quasicrystals*: *A Primer*, 2nd ed.; Oxford University Press: Oxford, U.K., 1994.
(4) Tsai, A. P. *MRS Bull.* **1997**, *22*, 43−47.
(5) Steurer, W. *Z. Kristallogr.* **1990**, *190*, 179−234.
(6) Yamamoto, A. *Acta Crystallogr., Sect. A*: *Found. Crystallogr.* **1996**, *A52*, 509−560.
(7) Fournee, V.; Belin-Ferre, E.; Sadoc, A.; Donnadieu, P.; Flank, A. M.; Muller, H. *J. Phys.: Condens. Matter* **1999**, *11*, 191−208.
(8) Bergman, G.; Waugh, J. L. T.; Pauling, L. *Nature* **1952**, *169*, 1057.
(9) Bergman, G.; Waugh, J. L. T.; Pauling, L. *Acta Crystallogr.* **1957**, *10*, 254.
(10) Cooper, M.; Robinson, K. *Acta Crystallogr.* **1966**, *20*, 614.
(11) Lee, C.-S.; Miller, G. J. *J. Am. Chem. Soc.* **2000**, *122*, 4937−4947.
(12) Elding-Ponten, M.; Lidin, S. *J. Solid State Chem.* **1995**, *115*, 270−273.
(13) Audier, M.; Pannetier, J.; Leblanc, M.; Janot, C.; Lang, J.-M.; Dubost, B. *Physica B* **1988**, *153*, 136.
(14) Tillard-Charbonnel, M.; Belin, C. *J. Solid State Chem.* **1991**, *90*, 270−278.
(15) Doering, W.; Seelentag, W.; Buchholz, W.; Schuster, H. U. *Z. Naturforsch., B*: *Anorg. Chem., Org. Chem.* **1979**, *34B*, 1715−1718.
(16) Todorov, E.; Sevov, S. C. *Inorg. Chem.* **1997**, *36*, 4298.

10.1021/ic0008363 CCC: $20.00 
Published on Web 12/08/2000

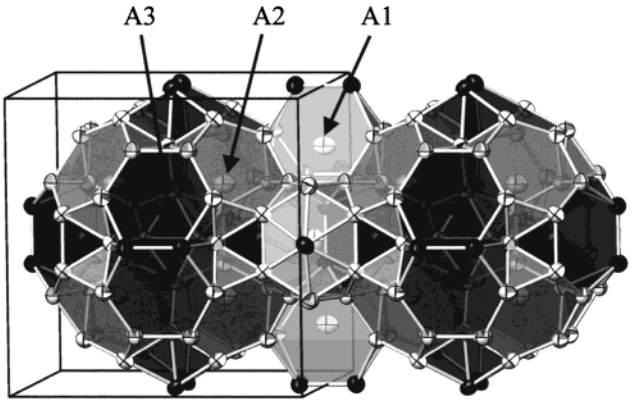


**Figure 1.** Crystal structure of the R-phase compound projected near [100]. The A1−A3 sites are drawn as isolated ellipsoids inside the clusters with different gray scales. White bonds connect Zn/Al atoms (M1−M4). The thermal ellipsoids are drawn at 99% probability from the data for $Li_{1.00(1)}Mg_{0.63(2)}Zn_{1.23(1)}Al_{2.14(1)}$ (**1**).

Sommerfeld model of tetrahedral semiconductors.[17] Therefore, the crystalline, cubic R-phase structure presents numerous possibilities for elemental site preferences and vacancy distributions in an intermetallic structure.

In this paper, we discuss a further theoretical study of the R-phase structure, revealing that the site potentials of the three A sites are not equal. This result prompted us to introduce other electropositive elements, such as Li, Ca, or Eu, into the Mg−Zn−Al system to form possible quaternary R-phases. To our knowledge, the only quaternary R-phase system to be reported is in the Na−Mg−Zn−Al system, but the relative site occupancies of Na, Mg, and Al atoms could not be definitely characterized because of their similar scatterings of X-rays. Our previous results obtained for the ternary Mg−Zn−Al R-phase system and the significant differences in X-ray scatterings between Mg and Li, Ca, or Eu make it possible to completely investigate the "coloring problem"[18] in this system of quasicrystalline approximants. Therefore, we also report the syntheses and the first single-crystal structural characterizations of ternary and quaternary R-phases in the Li−Zn−Al and Li−Mg−Zn−Al systems.

## The Theoretical Model

Before we discuss the theoretical model of site potentials in the R-phase species, we show its beautiful structure in Figure 1.[19] According to crystallographic studies on diverse intermetallic systems adopting the R-phase structure, four distinct positions (M1−M4 sites) create a network of pentagonal pyramids, icosahedra, and buckminsterfullerene-type clusters (truncated icosahedra) and three other positions (A1−A3 sites) fill interstices in the M1−M4 network. The coordination environments of the three A sites are shown in Figure 2. Environments for A2 (Wyckoff site 16f) and A3 (Wyckoff site 24g) are Friauf polyhedra, which are common structural elements in binary Mg−Zn and Mg−Al systems.[20,21] The four hexagonal faces are all capped by other A-site atoms. Eight A2 and twelve A3 environments fuse to form the "Samson polyhedron",[22] which contains 84 M atoms from a central icosahedron surrounded by twelve pentagonal pyramids. Adjacent Samson polyhedra share hexagons along {111} directions and M4−M4 edges along {100} directions to create the condensed, body-centered cubic packing of these building blocks.

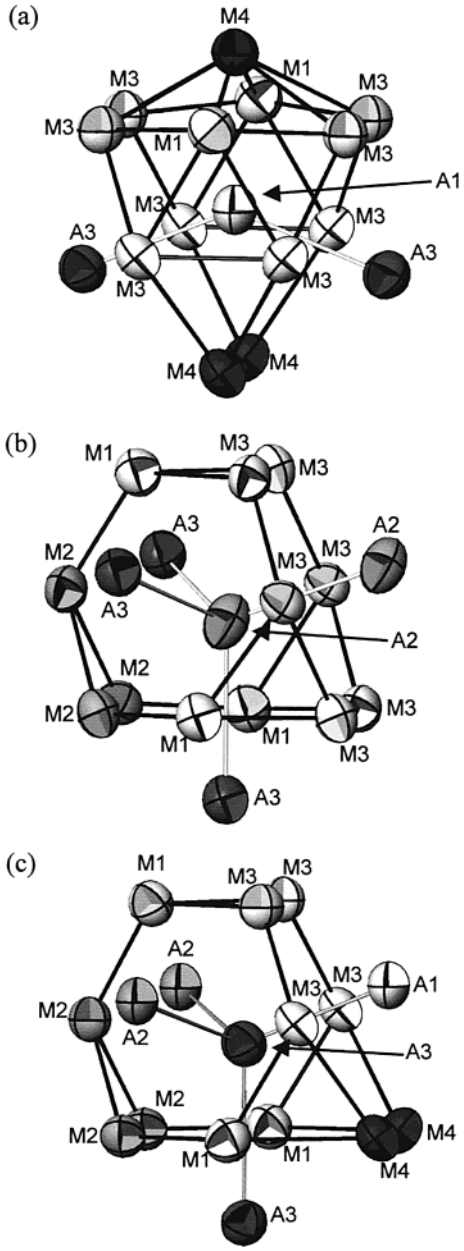


**Figure 2.** Three coordination environments for the A atoms in the R-phase structure. The thermal ellipsoid parameters are taken from the data for $Li_{1.00(1)}Mg_{0.63(2)}Zn_{1.23(1)}Al_{2.14(1)}$ (**1**). Gray bonds identify the shortest A−A contacts. (a) A1 type: 13-vertex cluster. (b) A2 type: truncated tetrahedron. (c) A3 type: truncated tetrahedron.

The environment surrounding each A1 site consists of 13 M atoms (2 M1 + 8 M3 + 3 M4 sites), with A3 atoms capping two hexagonal faces and an M4 site capping the third hexagonal face, as shown in Figure 2a. This particular interstitial site connects four adjacent Samson polyhedra in a tetrahedral arrangement—these sites are the tetrahedral holes in a bcc packing.[14]

(17) Burdett, J. K. *Molecular Shapes*: *Theoretical Models of Inorganic Stereochemistry*; Wiley: New York, 1980.
(18) Miller, G. J. *Eur. J. Inorg. Chem.* **1998**, 523−536.
(19) Dowty, E. *Atoms*, Version 5.0; 1999.
(20) Friauf, J. B. *Phys. Rev. B* **1927**, *29*, 34−40.
(21) Friauf, J. B. *J. Am. Chem. Soc.* **1927**, *49*, 3107−3114.
(22) Samson, S. In *Structure Chemistry and Molecular Biology*; Rich, A., Davidson, N., Eds.; Freeman: San Francisco, CA, 1968; pp 687−717.

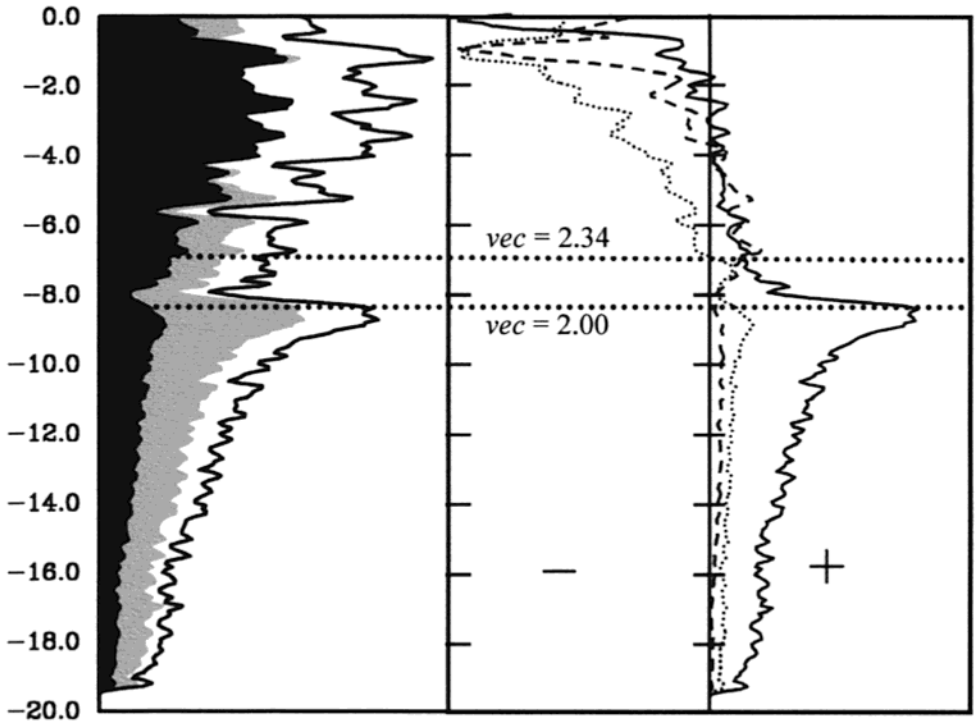


**Figure 3.** DOS and COOP curves from the model formula of $[Al_{26}][Al_{54}]$ for the R-phase. The two dotted lines denote the Fermi energies corresponding to the observed vec range in the Li−Mg−Zn−Al R-phases. Left: Total DOS (solid line), PDOS from A1−A3 sites (black shading), and PDOS from M1−M4 sites (gray shading). Right: COOP curves from contacts of A−A (dashed), A−M (dotted), and M−M (solid).

To study the site preference problem in R-phase compounds, extended Hückel tight-binding band calculations were performed on a model in which all seven crystallographic sites[23−26] were assigned the same atomic orbital parameters (Al). The primitive unit cell containing 80 atoms was used, and a special-points set of 60K points in the irreducible wedge of the first Brillouin zone of a bcc lattice was chosen to perform the integrations[27] for calculations of Mulliken populations, total and partial densities of states (DOS and PDOS), crystal orbital overlap populations (COOP's), and Fermi energies.[28,29] Atomic orbital parameters for Al are $H_{ii}(3s) = -12.3$ eV, $H_{ii}(3p) = -6.5$ eV, and $\zeta(3s) = \zeta(3p) = 1.167$.

The total DOS and the COOP curves for M−M, A−M, and A−A interactions are illustrated in Figure 3 for the model described above. The contributions to the total density of states (PDOS) curves from the M1−M4 and A1−A3 sites are represented respectively by gray and black areas. Two Fermi energies ($E_F$) are marked by dashed lines and represent the observed range in vec for R-phase structures: $2.00 \leq \text{vec} \leq 2.34$. The DOS curve shows a significant drop in the number of electronic states between −5.8 and −8.0 eV ($2.10 < \text{vec} < 2.70$), but no band gap occurs in this energy region. Furthermore, the relative contributions of orbitals from the M1−M4 and the A1−A3 sites are essentially equal in this region of the DOS. On the other hand, the M1−M4 orbitals have greater contributions at lower (occupied) energies ($E < -8.0$ eV), while the A1−A3 orbitals have larger contributions at higher (unoccupied) energies ($E > -6.0$ eV). Therefore, the density of valence electrons on the M1−M4 network is greater than that on the A1−A3 sites on the basis of the characteristics of the occupied energy bands in the R-phase. Since this calculation was carried out with the same atomic orbital parameters at each site in the structure, the resulting Mulliken populations are affected by the atomic coordination environment and the strengths of the various interatomic orbital interactions.

The COOP curves for A···A (dashed line), A−M (dotted line), and M−M (solid line) contacts are illustrated in Figure 3. For $2.00 \leq \text{vec} \leq 2.25$, the integrated overlap population of each contact is essentially optimized, since the orbital interactions for all metal−metal contacts in this region of the DOS are nearly nonbonding. Moreover, since there are electronic states contributing to this nonbonding region, R-phases should be metallic conductors. These COOP curves also suggest that the total strength of all chemical bonds in the R-phase structure is weakly sensitive to vec values in the range between 2.00 and 2.50 and that unit cell sizes will be controlled by the average atomic sizes rather than by special chemical bonding forces.

To elucidate the site potentials for the different crystallographic positions in the R-phase framework, we can compare the calculated Mulliken populations for these crystallographic sites. These results are plotted in Figure 4 as the relative Mulliken population for each independent crystallographic site vs total vec over a range of vec values in which the R-phase structure is observed for ternary and quaternary systems (indicated by the two dotted lines). The relative Mulliken population for a site equals the difference between the average vec and the calculated Mulliken population for that site. The extended Hückel method allows such an analysis because the energy DOS is constructed solely from atomic orbital interactions; valence electrons are then placed in these crystal orbitals according to the aufbau principle, and several different electron

(23) Hoffmann, R.; Lipscomb, W. N. *J. Chem. Phys.* **1962**, *36*, 2179, 3489.
(24) Hoffmann, R. *J. Chem. Phys* **1963**, *39*, 1397.
(25) Ammeter, J. H.; Buergi, H. B.; Thibeault, J. C.; Hoffmann, R. *J. Am. Chem. Soc.* **1978**, *100*, 3686−3692.
(26) Whangbo, M.-H.; Hoffmann, R.; Woodward, R. B. *Proc. R. Soc. London, Ser. A* **1979**, *366*, 23−46.
(27) Chadi, D. J.; Cohen, M. L. *Phys. Rev. B* **1973**, *8*, 5474.
(28) Hughbanks, T.; Hoffmann, R. *J. Am. Chem. Soc.* **1983**, *105*, 3528−3537.
(29) Wijeyesekera, S. D.; Hoffmann, R. *Organometallics* **1984**, *3*, 949−961.

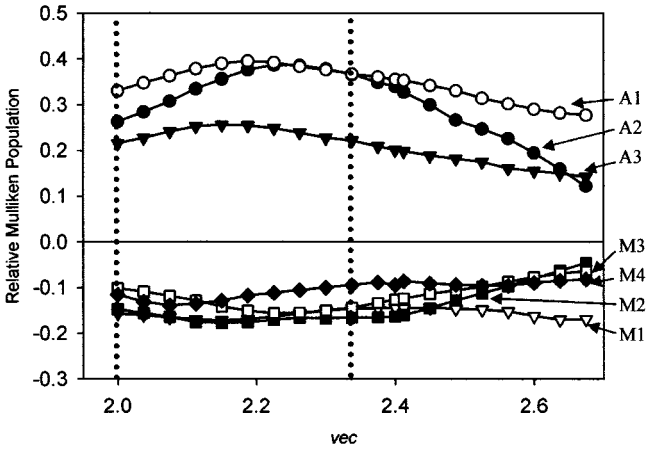


**Figure 4.** Relative Mulliken populations of the A1−A3 and M1−M4 sites as functions of the vec range from 2.0 ("$Mg_{52}Zn_{108}$") to 2.68 ("$Mg_{52}Al_{108}$"). The two dotted lines indicate the lower and higher limit of vec for ternary and quaternary Li−Mg−Zn−Al R-phases. A1: filled circle. A2: empty circle. A3: filled inverse triangle. M1: empty inverse triangle. M2: filled square. M3: empty square. M4: filled diamond.

counts can be examined. For a given vec, a positive (negative) value of the relative Mulliken population means an atomic site is positively (negatively) polarized. According to the concept of topological charge stabilization in a chemical structure with nonequivalent positions,[30] the atomic sites with high Mulliken populations (negative relative Mulliken populations) are favored for the more electronegative atoms and the sites with low Mulliken populations (positive relative Mulliken populations) are favored for the more electropositive atoms. Figure 4 shows some important features:

(1) The relative charges of the seven crystallographic sites can be divided into two groups. The M1−M4 sites are negatively polarized, and the A1−A3 sites are positively polarized. This is consistent with the relative electronegativities of the elements found on these two sets of positions for various ternary R-phase materials listed in Table 1: more electronegative elements occupy the M1−M4 sites.

(2) The A3 site shows significantly lower positive charge than both the A1 and A2 sites, suggesting that two different electropositive metallic elements may occupy the A1−A3 sites in a nonrandom fashion. In this case, the more electropositive atoms would preferentially segregate to the A1 and A2 positions in the R-phase structure.

(3) In the case of the M1−M4 sites, the M4 site is the least negatively polarized (closest to zero) when $2.12 \leq \text{vec} \leq 2.50$ and there is a crossover point between M4 and M3 when vec $= 2.12$. Our previous studies on the ternary Mg−Zn−Al R-phase system indicated that Zn and Mg atoms as well as vacancies occurred at the M4 position for higher Al content (vec $\geq 2.28$).

These theoretical results, especially points 2 and 3, prompted us to investigate various quaternary derivatives of the R-phase structure in the Mg−Zn−Al system by introducing other electropositive elements into the reactant mixture. We limited our scope to monovalent and divalent elements, i.e., alkali metal, alkaline earth metal, and divalent rare earth elements (Eu and Yb), and performed initial trials with those elements that were closest to Mg in size and electronegativity. We avoided Na because it would be difficult to differentiate Na from Mg using diffraction techniques. Among these elements, Eu is closest in electronegativity to Mg and Li is closest in atomic radius to Mg. Therefore, to take into account potential size and electrochemical effects, our targets involved quaternary systems with Li, Ca, and Eu. Size seemed to play a decisive role; also significant were the competing thermodynamic stabilities of binary aluminides, e.g., $CaAl_4$ and $EuAl_4$, which contributed to the result that Li was the only element among these three that would form new quaternary derivatives of the R-phase structure.

(30) Gimarc, B. M. *J. Am. Chem. Soc.* **1983**, *105*, 1979−1984.

## Experimental Studies of Quaternary Li−Mg−Zn−Al R-Phases

**Synthesis.** All materials were handled in an Ar-filled glovebox in which the concentration of $O_2$ was lower than 10 ppm. Starting materials included Li ingots (Johnson-Matthey, 99.5%), Mg turnings (Johnson-Matthey, 99.98%), Zn powder (Alfa, 99.9%), Al ingots (Alfa, 99.9999%), and Al foil. Maximum weighing errors were less than 1%. All reactant mixtures were sealed in cleaned Ta tubes (Alfa, 99.99%; washed with 15% HF/35% $HNO_3$/50% $H_2SO_4$ solution and dried) that were placed in evacuated, fused-silica Schlenk tubes. The ampules were heated to 1070−1120 K for 6 h, then cooled to 670 K at a rate of 5 K/h, and finally cooled to room temperature to quench the reactions. Several different reactant mixtures were designed and measured to give targets of $(Li_uMg_{1-u})_{52}(Zn_xAl_{1-x})_{108}$, $0 < u \leq 1$. These reactions are summarized in Table 2. All products were silvery and brittle, and sensitivity to moisture and air increased as the Li content increased. Reaction products were characterized by Guinier X-ray powder patterns using Cu Kα radiation ($\lambda = 1.540\,56$ Å). In all but one situation, reaction f, the R-phase structure was the major crystalline product, although subsequent single-crystal diffraction showed that there were subtle differences between the composition of the R-phase and the reactant composition. Reaction f produced a novel intermetallic structure, which will be reported elsewhere.[31]

**Single-Crystal X-ray Diffraction.** Single crystals suitable for X-ray diffraction analysis were selected from small amounts of crushed products. Crystals in the Li−Mg−Zn−Al system showed needlelike morphologies and were mounted on the tips of glass fibers. Crystal quality was checked by rotation photographs on a Siemens P4 single-crystal diffractometer with Mo Kα radiation ($\lambda = 0.710\,73$ Å) at room temperature (298(2) K). Diffraction data for detailed structural analyses were collected at 298(2) K using a Bruker CCD-1000 diffractometer with monochromatic Mo Kα radiation and a detector to crystal distance of 5.08 cm. At least two independent single-crystal data sets were collected for each sample. For each crystal, the data were collected in at least a quarter hemisphere and harvested by collecting three sets of frames with 0.3° scans in $\omega$ for an exposure time of 30−60 s per frame. The range of $2\theta$ values was 3.0−58.0°. The data were corrected for Lorentz and polarization effects. Absorption corrections were based on fitting a function to the empirical transmission surface as sampled by multiple equivalent measurements. The unit cell parameters were determined from 90 frames of reciprocal space images and then least-squares-refined with all observed intensity data. Structures were solved by direct methods (SHELXTL-V5.12[32,33]) and subsequently refined by full-matrix least-squares calculations based on $F^2$ using a model based upon $Mg_{1.63}(Zn_xAl_{1-x})_{3.37}$.[34] An abbreviated summary of the crystallographic data is given in Table 3. Detailed crystallographic data, atomic positions, site occupancies, and internuclear separations for all compounds are available as Supporting Information.

**Magnetic Susceptibility Measurements.** Magnetic susceptibility measurements were carried out at 3T using a Quantum Design SQUID magnetometer for the products of reactions d and i (Table 2), $Li_{1.00}Mg_{0.63}Zn_{1.22}Al_{2.15}$ (5−260 K) and $Li_{1.63}Zn_{1.50}Al_{1.87}$ (5−150 K). After diamagnetic core corrections, both compounds show temperature

(31) Lee, C.-S.; Miller, G. J. Manuscript in preparation.

(32) Sheldrick, G. M. *SHELXTL: Structure Determination Programs*, Version 5.12; Siemens Analytical X-ray Instruments Inc.: Madison, WI, 1995.

(33) *SAINT*, Version 4; Siemens Analytical X-ray Instruments Inc.: Madison, WI, 1995.

(34) Sheldrick, G. M. In *Crystallographic Computing 3*; Sheldrick, G. M., Kruger, C., Goddard, R., Eds.; Oxford University Press: Oxford, U.K., 1985; p 175.

**Table 1.** Summary of Known R-Phases with the Site Preference on Each Atomic Site

| formula | *a*, Å | MO[b] 2a | M1 24c | M2 24b | M3 48f | M4 12g | A1 12h | A2 16d | A3 24e | ref |
|---|---|---|---|---|---|---|---|---|---|---|
| $Mg_{32}(Zn,Al)_{49}$ | 14.16(3) | Al | Zn/Al | Zn/Al | Zn/Al | Mg | Mg | Mg | Mg | 11 |
| $Mg_{1.63}(Zn,Al)_{3.37}$ | 14.13−14.41 | | Zn/Al | Zn/Al | Zn/Al | Mg/Zn/Al | Mg | Mg | Mg | 11 |
| $(Li,Mg)_{1.63}(Zn,Al)_{3.37}$ | 13.93−14.10 | | Zn/Al | Zn/Al | Zn/Al | Zn/Al | Li | Li/Mg | Li/Mg | *a* |
| $Li_{1.63}(Zn,Al)_{3.37}$ | 13.93−14.14 | | Zn/Al | Zn/Al | Zn/Al | Al | Li | Li | Li | *a* |
| $Li_{52}Ni_{37}Si_{72}$ | 12.741 | | Ni/Si | Ni/Si | Ni/Si | Ni/Si | Li | Li | Li | 15 |
| $Li_{52}Cu_{57}Si_{51}$ | 12.933 | | Cu/Si | Cu/Si | Cu/Si | Cu/Si | Li | Li | Li | 15 |
| $Li_{13}Cu_6Ga_{21}$ | 13.568(2) | | Cu | Ga | Ga | Ga | Li | Li | Li | 14 |
| $Li_3CuAl_5$ | 13.9056(3) | | Cu/Al | Cu/Al | Cu/Al | Al | Li | Li | Li | 13 |
| $Na_{52}Au_{81}Si_{29}$ | 14.138 | Au | Si | Au | Au | Au/Si | Na | Na | Na | 15 |
| $Mg_{36}Na_{16}Zn_{68}Al_{40}$ | 14.2173(7) | | Zn/Al | Zn/Al | Zn/Al | Al | Mg/Na | Mg/Na | Mg/Na | 12 |
| $Na_{52}Au_{80}Ge_{30}$ | 14.620 | Au | Ge | Au | Au | Au/Ge | Na | Na | Na | 15 |
| $Na_{15}Au_{17}Sn_6$ | 14.989 | Au | Sn | Au | Au | Au/Na | Na | Na | Na | 15 |
| $Na_{13}Cd_{20}Pb_7$ | 15.992(2) | | Cd | Cd/Pb | Cd/Pb | Cd/Pb | Na | Na | Na | 16 |

[a] This work. [b] Wyckoff site 2a (0, 0, 0).

**Table 2.** Labeled Summary of Reaction Compositions and Products Identified by Guinier X-ray Powder Diffraction and Single-Crystal X-ray Diffraction Measurements for Various Li−Mg−Zn−Al Reactions

| reaction | vec | unit cell (*a*, Å)[b] | identified minor phase(s)[a] | refined formula[d] | vec |
|---|---|---|---|---|---|
| 1. $(Li_xMg_{1-x})_{1.63}(Zn_yAl_{1-y})_{3.37}$ | | | | | |
| (a) $Li_{0.88}Mg_{0.75}Zn_{1.13}Al_{2.24}$ | 2.272 | 14.073(3) | $MgZn_2$(t) + $Mg_2Zn_{11}$(t) + Al(t) | $Li_{1.00(1)}Mg_{0.63(2)}Zn_{1.23(1)}Al_{2.14(1)}$ (**1**) | 2.23(2) |
| (b) $Li_{0.88}Mg_{0.75}Zn_{1.13}Al_{2.24}$ | 2.272 | 14.088(3) | Al(t) + Zn(t) | $Li_{1.00(1)}Mg_{0.63(1)}Zn_{1.42(1)}Al_{1.96(1)}$ (**2**) | 2.20(2) |
| (c) $Li_{0.63}Mg_{1.00}Zn_{1.22}Al_{2.15}$ | 2.304 | 14.096(5) | NA[e] | $Li_{1.01(1)}Mg_{0.62(1)}Zn_{1.31(1)}Al_{2.06(1)}$ (**3**) | 2.21(2) |
| (d) $Li_{1.00}Mg_{0.63}Zn_{1.22}Al_{2.15}$ | 2.230 | 13.993(5) | NA | $Li_{1.03(1)}Mg_{0.60(1)}Zn_{1.78(3)}Al_{1.59(3)}$ (**4**) | 2.11(4) |
| (e) $Li_{0.63}Mg_{1.00}Zn_{2.66}Al_{0.71}$ | 2.016 | 13.933(3) | $MgZn_2$(t) + $Mg_2Zn_{11}$(t) + Al(t) | $Li_{0.78(2)}Mg_{0.85(2)}Zn_{2.47(1)}Al_{0.94(1)}$ (**5**) | 2.05(2) |
| (f) $Li_{1.00}Mg_{0.63}Zn_{2.66}Al_{0.71}$ | 1.942 | 13.951(4) | R−Phase (m) + Al(t) | $Li_{1.00(2)}Mg_{0.60(2)}Zn_{3.09(1)}Al_{0.31(1)}$[c] | 1.86(2) |
| 2. $Li_{1.63}(Zn_xAl_{1-x})_{3.37}$ | | | | | |
| (g) $Li_{1.63}Zn_{1.00}Al_{2.37}$ | 2.148 | 14.135(3) | LiZn(t) + LiAl(t) + Al(t) | $Li_{1.63}Zn_{0.81(1)}Al_{2.56(1)}$ (**6**) | 2.19(1) |
| (h) $Li_{1.63}Zn_{1.22}Al_{2.15}$ | 2.104 | 13.966(5) | NA | $Li_{1.63}Zn_{1.42(1)}Al_{1.95(1)}$ (**7**) | 2.19(1) |
| (i) $Li_{1.63}Zn_{1.50}Al_{1.87}$ | 2.048 | 13.947(2) | NA | $Li_{1.63}Zn_{1.59(1)}Al_{1.78(1)}$ (**8**) | 2.03(1) |
| (j) $Li_{1.63}Zn_{2.25}Al_{1.17}$ | 1.928 | 13.933(4) | Zn(t) | $Li_{1.63}Zn_{1.77(1)}Al_{1.60(1)}$ (**9**) | 1.99(1) |

[a] From Guinier powder patterns; m = minor phase, t = trace amount. [b] From Guinier powder X-ray diffractions. [c] Reference 31. [d] From single-crystal refinements. [e] Not applicable.

**Table 3.**

(a) Crystallographic Data for the Five Quaternary Samples $Li_{1.00(1)}Mg_{0.63(2)}Zn_{1.23(1)}Al_{2.14(1)}$ (**1**), $Li_{1.00(1)}Mg_{0.63(1)}Zn_{1.42(1)}Al_{1.96(1)}$ (**2**), $Li_{1.01(1)}Mg_{0.62(1)}Zn_{1.31(1)}Al_{2.06(1)}$ (**3**), $Li_{1.03(1)}Mg_{0.60(1)}Zn_{1.78(3)}Al_{1.59(3)}$ (**4**), and $Li_{0.78(2)}Mg_{0.85(2)}Mg_{0.85(2)}Zn_{2.47(1)}Al_{0.94(1)}$ (**5**), from Single-Crystal X-ray Diffraction Measurements

| | **1** | **2** | **3** | **4** | **5** |
|---|---|---|---|---|---|
| fw | 160.16 | 167.63 | 163.26 | 181.51 | 211.44 |
| space group, *Z* | *Im*$\bar{3}$, 32 | *Im*$\bar{3}$, 32 | *Im*$\bar{3}$, 32 | *Im*$\bar{3}$, 32 | *Im*$\bar{3}$, 32 |
| *a*,[a] Å | 14.073(3) | 14.088(3) | 14.096(5) | 13.993(5) | 13.933(2) |
| *V*, Å[a] | 2787.1(5) | 2807.0(4) | 2801.8(7) | 2806.2(6) | 2699.3(8) |
| $\lambda$(Mo K$\alpha$), Å | 0.710 73 | 0.710 73 | 0.710 73 | 0.710 73 | 0.710 73 |
| temp, K | 293(2) | 293(2) | 293(2) | 293(2) | 293(2) |
| $\mu$, cm$^{-1}$ | 8.893 | 10.116 | 9.416 | 12.501 | 17.478 |
| $d_{calc}$, g/cm$^3$ | 3.040 | 3.173 | 3.096 | 3.437 | 4.162 |
| R1, wR2 [$I > 2\sigma(I)$][b] | 0.0224, 0.0307 | 0.0194, 0.0348 | 0.0169, 0.0295 | 0.0157, 0.0385 | 0.0240, 0.0498 |
| R1, wR2 (all data)[b] | 0.0381, 0.0322 | 0.0272, 0.0360 | 0.0229, 0.0305 | 0.0178, 0.0391 | 0.0304, 0.0517 |

(b) Crystallographic Data for the Four Ternary Samples $Li_{1.63}Zn_{0.81(1)}Al_{2.56(1)}$ (**6**), $Li_{1.63}Zn_{1.42(1)}Al_{1.95(1)}$ (**7**), $Li_{1.63}Zn_{1.59(1)}Al_{1.78(1)}$ (**8**), and $Li_{1.63}Zn_{1.77(1)}Al_{1.60(1)}$ (**9**), from Single-Crysal X-ray Diffraction Measurements

| | **6** | **7** | **8** | **9** |
|---|---|---|---|---|
| fw | 133.53 | 157.22 | 163.76 | 179 |
| space group, *Z* | *Im*$\bar{3}$, 32 | *Im*$\bar{3}$, 32 | *Im*$\bar{3}$, 32 | *Im*$\bar{3}$, 32 |
| *a*,[a] Å | 14.135(3) | 13.966(5) | 13.947(2) | 13.933(4) |
| *V*, Å[a] | 2759.4(1) | 2721.1(5) | 2717.3(6) | 2704.4(5) |
| $\lambda$(Mo K$\alpha$), Å | 0.710 73 | 0.710 73 | 0.710 73 | 0.710 73 |
| temp, K | 293(2) | 293(2) | 293(2) | 293(2) |
| $\mu$, cm$^{-1}$ | 6.206 | 10.381 | 11.525 | 12.727 |
| $d_{calc}$, g/cm$^3$ | 2.571 | 3.070 | 3.202 | 3.347 |
| R1, wR2 [$I > 2\sigma(I)$][b] | 0.0247, 0.0376 | 0.0199, 0.0367 | 0.0262, 0.0453 | 0.0176, 0.0306 |
| R1, wR2 (all data)[b] | 0.0429, 0.0395 | 0.0277, 0.0374 | 0.0421, 0.0474 | 0.0262, 0.0314 |

[a] From Guinier powder patterns (298(2) K). [b] $R1 = \sum||F_o| - |F_c||/\sum|F_o|$; $wR2 = [\sum w(F_o^2 - F_c^2)^2/\sum w(F_o^2)^2]^{1/2}$, $w = \sigma_F^{-2}$.

independent susceptibilities above ca. 50 K. $Li_{1.00}Mg_{0.63}Zn_{1.22}Al_{2.15}$ exhibits paramagnetic behavior and the average magnetic susceptibility above 50 K is $8.51 \times 10^{-6}$ emu/mol. On the other hand, $Li_{1.63}Zn_{1.50}Al_{1.87}$ shows diamagnetic behavior and the average susceptibility above 50 K is $-1.9 \times 10^{-4}$ emu/mol.

## Results and Discussion

Compositions, structures, site occupancies, and properties of intermetallic compounds in general are closely interrelated aspects of such species and really cannot be considered

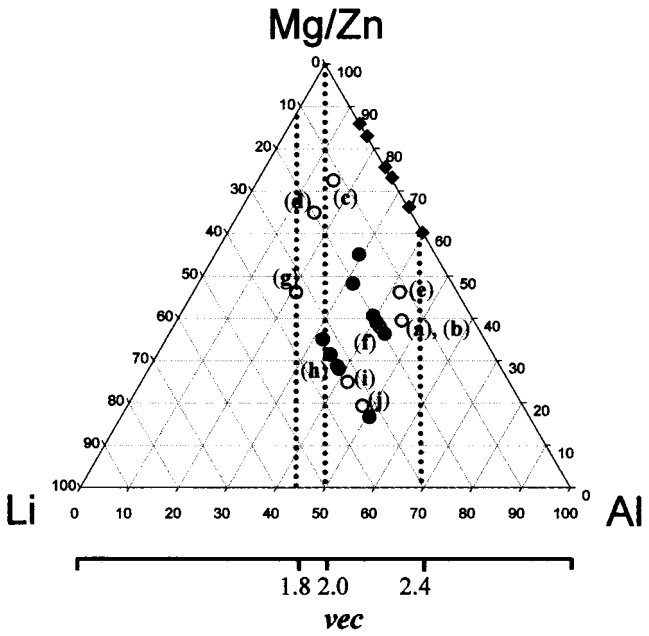


**Figure 5.** Phase diagram representing various ternary and quaternary Li−Mg−Zn−Al reactions (open circles, reactions a−j, see Table 1) and refined compositions (filled circles). Filled diamonds are single-crystal results from ternary Mg−Zn−Al R-phase compounds.

separately. Nevertheless, to facilitate the discussion of our results, we will address each aspect in its own section and conclude with an overview of these relationships.

**Compositions in Li−Mg−Zn−Al R-Phases.** Figure 5 summarizes the compositional results in a pseudoternary (isothermal) phase diagram based upon vec. Different starting compositions involving five quaternary mixtures (reactions a−f, Table 1) and four ternary Li−Zn−Al mixtures (reactions g−j, Table 1) are indicated by open circles in the diagram. Compositions based upon refinements of site occupancies from single-crystal X-ray diffraction experiments are shown by filled circles on the same diagram. Although starting compositions give a range in vec from ca. 1.8 to 2.3, the single-crystal results produced a narrower range between 2.00 and 2.25, which is in excellent agreement with our findings from electronic structure calculations. The observed minimum vec value requires that the maximum Li/Al ratio be 1.0. Also, the maximum Li content is 0.325, which is exactly in accord with 52 A sites per unit cell.

**Structures and Site Occupancies in Li−Mg−Zn−Al R-Phases.** The positional parameters and site occupancies for the structures of quaternary Li−Mg−Zn−Al crystals were first refined by placing Mg atoms on the A1−A3 sites and Al atoms on the M1−M4 sites and fixing isotropic thermal displacement parameters. After a few cycles of least-squares refinements, the site occupancies indicated that the A1−A3 sites (Wyckoff sites 12h and 16d) were electron deficient compared to Mg and should be partially occupied by Li. On the other hand, the refined electron densities on the M1−M4 sites were larger than that on Al and should be refined as a mixture of Zn and Al. Once the possible atom types were determined for each site, subsequent refinements included anisotropic displacement parameters.

Figures 6 and 7 illustrate results concerning structures and site occupancies of quaternary and ternary R-phase systems. Parts a and b of Figure 6 show the correlations between unit cell volumes and, average atomic volume and vec, respectively. Included in these graphs are results from our earlier work with ternary Mg−Zn−Al R-phases.[11] Clearly, the unit cell volumes

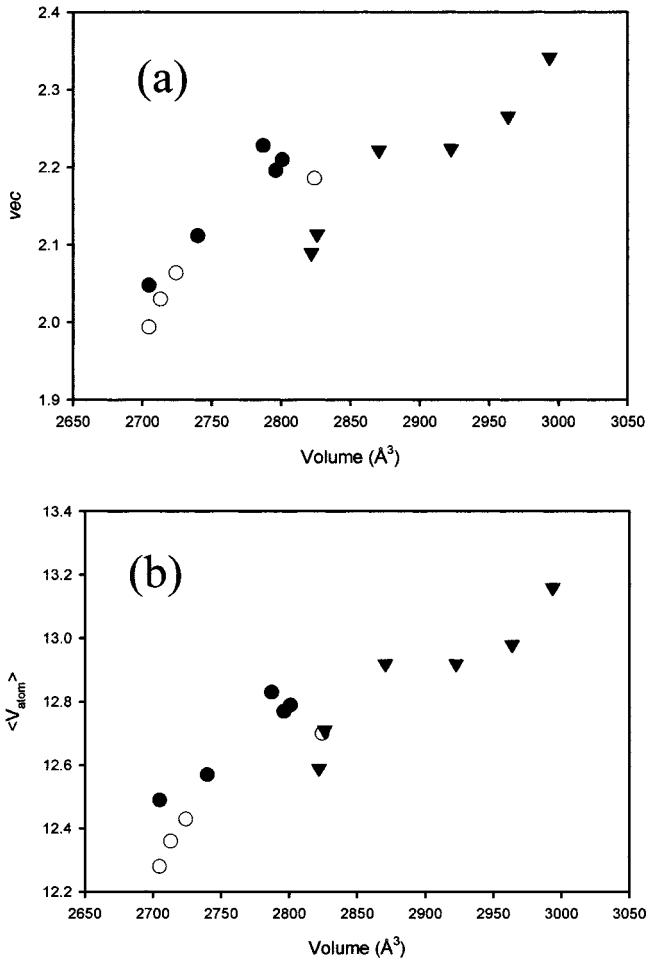


**Figure 6.** (a) Vec and (b) average atomic volume vs cell volume (Å$^3$) for ternary and quaternary R-phase systems. Filled circles: Li−Mg−Zn−Al. Empty circles: Li−Zn−Al. Filled inverse triangles: Mg−Zn−Al.

increase as both the average size and electron count of the component elements increase. Although the correlation with average atomic volume is clear, the correlation with vec requires some explanation. Throughout the range of observed vec values (2.00−2.35 for all examples in Figure 6), the orbitals near the corresponding Fermi levels show an overall nonbonding character with respect to M−M, A−M, and A−A contacts (see COOP curves in Figure 3). Therefore, the trend in unit cell volume should follow the changes in atomic volumes associated with the elements controlling the vec. In the ternary classes of R-phases, i.e., the Li−Zn−Al and Mg−Zn−Al systems, vec values increase as the Al/Zn stoichiometric ratio increases. Since the metallic radius of Al (1.43 Å) exceeds that of Zn (1.34 Å), as vec increases in these two systems, the average atomic volume increases and the unit cell volume also increases. For the quaternary Li−Mg−Zn−Al system, crystallographic experiments demonstrated that the Li/Mg stoichiometric ratio also did not change. Thus, again, vec values increase as the Al/Zn ratio increases and the same trend will occur.

Site occupancies among the different A and M sites in the quaternary crystals also show interesting variations. Figure 7a reveals the Li site occupancies at the three different A sites in the quaternary systems. The A1 site is completely occupied by Li, whereas the A2 and A3 sites are occupied by a mixture of Li and Mg. Since the experimental vec values in the Li−Mg−Zn−Al system lie between 2.00 and 2.25 e$^-$/atom, the relative site occupancies follow theoretical expectations for the three A

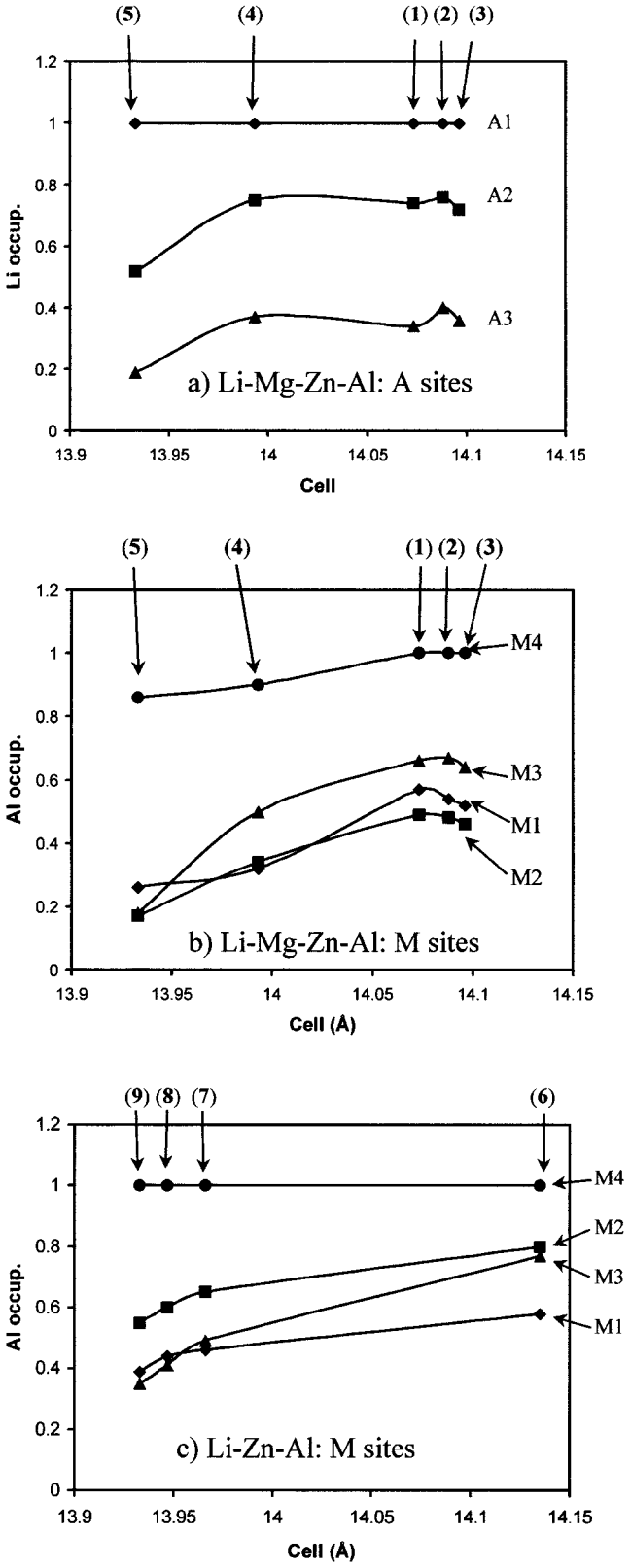


**Figure 7.** Relationship between site occupancies (Li, A sites; Al, M sites) and unit cell constants (Å) for ternary and quaternary R-phase compounds.

sites exactly (see Figure 4). The A2 and A3 sites constitute pentagonal dodecahedra that cap the faces of the internal icosahedra (M2 sites) in the Samson cluster. Parts b and c of Figure 7 illustrate how the Al contents vary among the crystals in the Li−Zn−Al and Li−Mg−Zn−Al systems. In all Li−Zn−Al crystals and in the quaternary system when vec is between

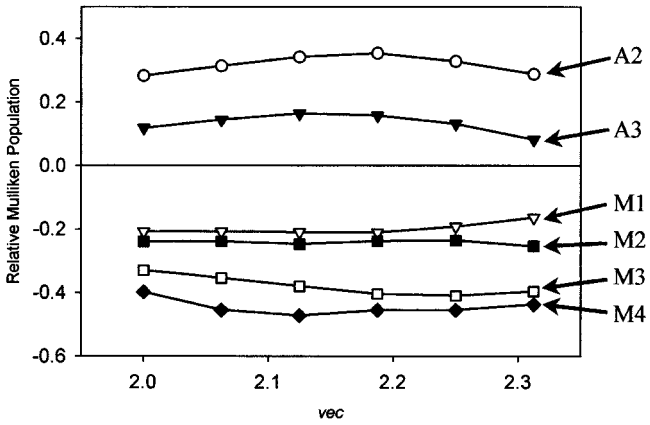


**Figure 8.** Relative Mulliken populations of A2, A3, and M1−M4 sites as a function of the vec range based on the model $(\square_{12}Al_{40})Al_{108}$. The *x* axis indicates the observed vec range for ternary and quaternary R-phases. A2: empty circle. A3: filled inverse triangle. M1: empty inverse triangle. M2: filled square. M3: empty square. M4: filled diamond.

ca. 2.15 and 2.25 $e^-$/atom, the M4 sites are exclusively occupied by Al atoms (there are no vacancies apparent in our refinements, which is consistent with our conclusions from the Mg−Zn−Al system that introduced vacancies into the M4 sites when vec exceeded 2.28 $e^-$/atom). When vec drops below 2.15 $e^-$/atom in the Li−Mg−Zn−Al crystals, a small amount of Zn also occupies each M4 site. All other M sites (M1, M2, and M3) show a monotonic increase in Al content with lattice constant for both systems. Unlike the case for the ternary Mg−Zn−Al systems, the Al content at the M2 sites varies among the different crystals.

The goal of replacing Mg with Li in the electronic structure of the R-phases is to introduce high-energy atomic orbitals at the Li sites. To investigate the change in site potentials throughout the R-phase structure, we treated the Li sites as vacant (i.e., no atomic orbitals were positioned at these sites, which is equivalent to placing a negative potential at these sites that repels electrons) but included its one valence electron in the total valence electron count. Figure 8 illustrates the variation in relative Mulliken populations with vec for the model $\square_{12}A_{40}M_{108}$ (A2, A3, and all M sites are given Al parameters; the A1 site is vacant). From this calculation, we observe the following results: (1) The M4 site clearly becomes the most negatively polarized and highly attractive for the Al atoms. Such sites are also not well suited to accommodate vacancies. (2) The A2 site is definitely more positively polarized than the A3 site. In the quaternary Li−Mg−Zn−Al crystals, the A2 site obtains significantly more Li than the A3 site, which agrees with these theoretical results.

## Conclusions

In this study, ternary and quaternary R-phases are characterized and the results reveal a nonrandom site preference for Li and Mg atoms among the A1−A3 sites in the structure. A Mulliken population analysis from extended Hückel tight-binding band calculations on the R-phase structure separates the atomic positions into two groups of positively and negatively polarized sites, whose site occupancies follow elemental electronegativities. The site potentials of different atomic positions depend on the various coordination environments and lead to a difference among the three "cation" sites, A1−A3. A subsequent X-ray diffraction study on quaternary samples indicates that Li more readily occupies the isolated A1 sites than the A2 and A3

positions that generate pentagonal dodecahedra. The behavior of the M1−M4 sites toward Zn/Al ratios are also affected by the Li atoms. The M1−M4 sites are all completely occupied, as the vec values remain below 2.25 $e^-$/atom for the quaternary examples. A previous study of the Mg−Zn−Al system revealed vacancies at the M4 site when vec exceeded 2.25 $e^-$/atom, and this work also showed that vec remained below 2.15 in the Li−Zn−Al R-phase system. Therefore, the additional flexibility in composition in the quaternary Li−Mg−Zn−Al crystals allowed the system to achieve an optimal valence electron concentration near 2.25 $e^-$/atom (360 electrons per unit cell; King cited 340 electrons per unit cell using simple electron-counting schemes.[35]). Theoretical calculations of the relative Mulliken populations for the different crystallographic sites in these intermetallic phases provide a beautiful model for predicting site preferences. These calculations can be used with X-ray diffraction data to provide models for structural refinements. We are currently applying this technique to related intermetallics and quasicrystalline phases.

**Acknowledgment.** This work was supported by NSF Grants DMR 96-27161 and DMR 99-81766. We are grateful to Dr. R. A. Jacobson for the use of the X-ray diffractometers, Dr. Ilia Guzei for training on the Bruker CCD-1000 diffractometer (which was purchased by NSF Grant 97-11121), and J. Ostenson for the magnetic susceptibility measurements.

**Supporting Information Available:** Tables of additional crystallographic data, atomic coordinates and *U*(eq) values, anisotropic displacement parameters, interatomic distances, and results of the powder X-ray unit cell refinements for compounds **1**−**9**, as well as a figure showing magnetic susceptibility as a function of temperature for "$Li_{0.88}Mg_{0.75}Zn_{1.13}Al_{2.34}$" and "$Li_{1.63}Zn_{1.50}Al_{1.87}$". This material is available free of charge via the Internet at http://pubs.acs.org.

IC0008363

(35) King, R. B. *Inorg. Chim. Acta* **1991**, *181*, 217−225.